Available online at www.sciencedirect.com

ScienceDirect

journal homepage: www.elsevier.com/locate/he

Model predictive control to ensure high quality hydrogen production for fuel cells

P. Rullo [a], L. Nieto Degliuomini [a], M. García [a], M. Basualdo [a,b,*]

[a] Computer Aided for Process Engineering Group (CAPEG), French–Argentine International Center for Information and Systems Sciences (CIFASIS-CONICET-UNR-UPCAM), 27 de Febrero 210 bis, S2000EZP Rosario, Argentina
[b] Universidad Tecnológica Nacional – FRRo, Zeballos 1341, S2000BQA Rosario, Argentina

ARTICLE INFO

Article history:
Received 8 October 2013
Accepted 6 December 2013
Available online 17 January 2014

Keywords:
Model predictive control
Bioethanol processor system
CO soft sensor
PEM quality hydrogen production

ABSTRACT

In this work, a conventional plant wide control of a hydrogen production process from bioethanol is analyzed. The objective is to determine if the carbon monoxide (CO), in the produced hydrogen, exceeds the Proton Exchange Membrane Fuel Cell quality requirement of 10 ppm. Commercial sensors that meet those process conditions at high temperature are not easily available. Then, the development of two soft sensors, based on neural network, for online estimation of CO concentration in the H_2 stream is presented. Higher CO concentration than allowed is detected in the fuel cell feeding. Strong interaction effects among the control loops around the last reactor, are found. Based on this, two model predictive control technologies are tested and compared in this interacted zone, in order to improve the disturbance rejection and satisfy the H_2 expected quality. An exigent disturbance profile was used for simulating dynamically the complete process behavior.

1. Introduction

The increasing reduction of fossil fuel reserves and the environmental degradation derived from their combustion have become major concerns of the current global energetic matrix. The progressive transition to all-electric vehicles powered by some combination of fuel cells and batteries is essential to begin solving the problems derived from the fossil fuel dependence [1]. Proton Exchange Membrane Fuel Cell (PEMFC), fed by hydrogen, is considered the best option for mobile applications due to its compactness, modularity, low temperature working point, higher conversion efficiencies and low emissions of pollutants and noise [2]. Hydrogen is not an expensive substance, but it is extremely dangerous to transport and store. Therefore an onboard processing system to produce this gas from liquid renewable materials, such as bioethanol, is a great replacement, given that it is much safer to manipulate, and the current refueling infrastructure is able to handle it [3]. The most typical raw materials used to produce bioethanol can be either primary crops (usually corn or soy) or residuals materials (lignocellulosic or sugar industry). The ethanol produced from agricultural products has a better energy balance, nevertheless this option competes with feed-oriented crops and encourages chemical intensive monoculture, with dangerous consequences for people [4,5]. There

* *Corresponding author*. Computer Aided for Process Engineering Group (CAPEG), French–Argentine International Center for Information and Systems Sciences (CIFASIS-CONICET-UNR-UPCAM), 27 de Febrero 210 bis, S2000EZP Rosario, Argentina. Tel.: +54 341 4237248 333; fax: +54 341 482 1772.
E-mail addresses: rullo@cifasis-conicet.gov.ar (P. Rullo), nieto@cifasis-conicet.gov.ar (L. Nieto Degliuomini), mgarcia@cifasis-conicet.gov.ar (M. García), basualdo@cifasis-conicet.gov.ar (M. Basualdo).
0360-3199/$ – see front matter Copyright © 2013, Hydrogen Energy Publications, LLC. Published by Elsevier Ltd. All rights reserved.
http://dx.doi.org/10.1016/j.ijhydene.2013.12.069

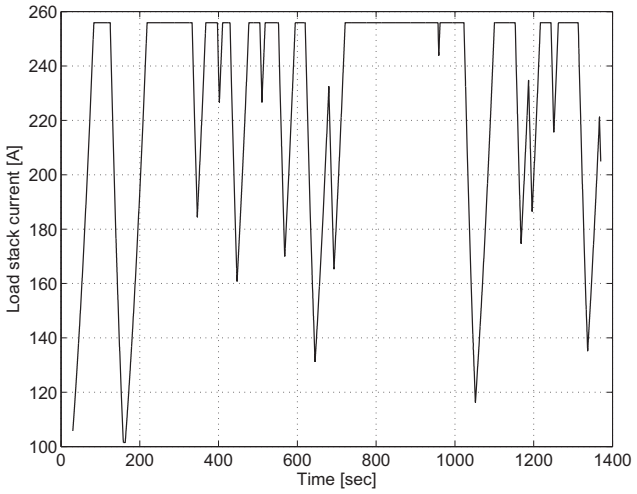

Fig. 1 – Load stack current profile (from UDDS).

are many ways to obtain hydrogen from hydrocarbons, among them the steam reforming is considered because high concentrations of hydrogen can be obtained [6]. The Bio-ethanol processor system (BPS) consists of an ethanol steam reformer (ESR), followed by a purification unit in order to reduce the CO concentration of the output stream below 10 ppm before feeding the PEM-FC. This is a critical issue to maintain high levels of efficiency on the system. The pseudo dynamic rigorous model of the BPS to produce hydrogen for the PEM-FC presented by Nieto Degliuomini et al. [7] is used in this work. It was modeled by using mass and energy balances, chemical equilibrium, thermodynamic models and feasible heat transfer conditions.

It has been shown that even relatively low levels of CO concentration in the H_2 rich stream can lead to significant performance degradation and eventually spontaneous oscillations in cell potential due to anode catalyst poisoning [8]. Therefore, an on-line measurement is essential for feedback control and safety purposes. There exist many commercial CO sensors, however, none of them is able to meet the

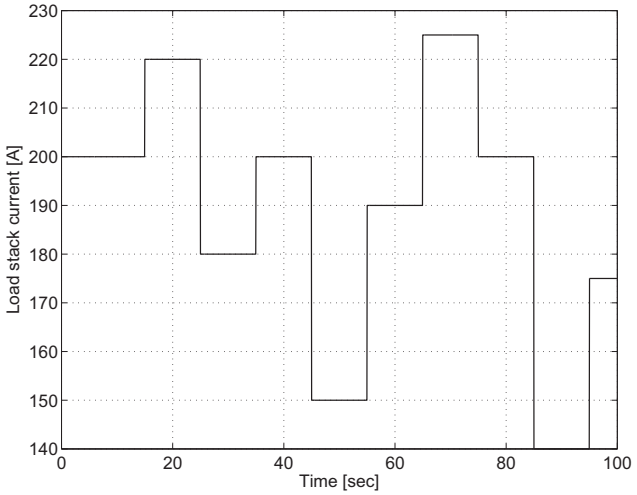

Fig. 2 – Load Stack current profile – Disturbance.

Table 1 – Variables in soft sensor 1.

Variable	Description
y_7 (Input)	LTS exit temperature
u_9 (Input)	LTS exit flow
$\widehat{y_9}$ (Predicted)	CO-PrOx CO inlet concentration

requirements of a PEM-FC based systems. Serious failings like cross-sensitivities, instability in high concentrations of hydrogen, high cost, limited temperature ranges or slow time responses make them unfeasible [9,10]. Research advances aimed at finding a solution to these problems are showed in Ref. [11].

Soft sensors (SS) provide an accurate alternative to hardware measurement equipments for on-line prediction of process variables which can be only determined with low sampling rates or through off-line analysis. Artificial neural networks (ANNs) have been shown to be an adequate modeling choice in order to deal with nonlinear systems and real-time operation [12]. Therefore they become an ideal choice for the predicting model of a CO soft sensor. This paper proposes the development of two ANN based soft sensors for the estimation of CO concentration in a H_2 rich stream. The first one is used in the estimation of oxygen to carbon monoxide ratio (O_2/CO) at the inlet of the oxidation unit since it is critical to maintain a good performance. The other is intended to monitor CO traces in the feeding of the PEM-FC. There are many studies in prediction, monitoring and control of process variables using ANN based soft sensors [13,14]. However, the use of them in monitoring CO concentration in PEM-FC based systems is non-existent. Soft sensors implementation allows the monitoring of important quality and security variables. However a proper definition of the control structure is essential to keep the overall system at the wanted operating point of high efficiency even in the presence of disturbances and satisfy the PEM quality hydrogen production (CO concentration $<$10 ppm).

This paper is based in the work presented by Nieto Degliuomini et al. [15]. They proposed a decentralized PI control structure with six loops through the implementation of a generalized methodology for plant-wide control [16–19]. All the control loops present a suitable dynamic behavior. Nevertheless, the transient response of the CO concentration at the feeding of the PEM-FC is not considered. The goal of this work is to propose two model predictive control (MPC) strategies replacing only the critical loops in order to improve the dynamic performances and satisfy the quality restriction in the H_2 stream. Based on the study of the relative gain array (RGA), the most interactive loops in the plant are identified and become candidates for substitution with an advanced SISO (Single Input–Single Output) or MIMO (Multiple

Table 2 – Variables in soft sensors 2.

Variable	Description
$\widehat{y_9}$ (Input)	CO-PrOx inlet CO concentration
u_9 (Input)	LTS exit flow
y_8 (Input)	CO-PrOx exit temperature
y_9 (Input)	Molar ratio O_2/CO
y_{11} (Predicted)	CO-PrOx CO outlet concentration

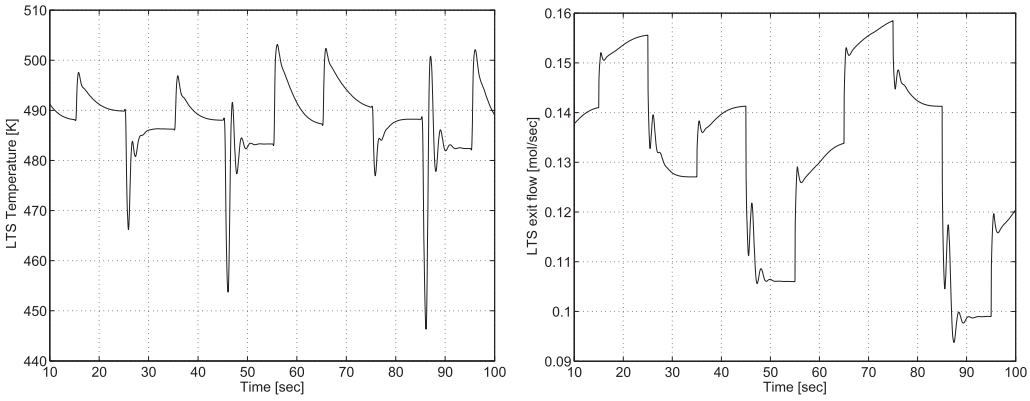

(a) Input 1 - y_7: LTS exit temperature (b) Input 2 - u_9: LTS exit flow

Fig. 3 – SS1 Training data – Input profiles.

Input–Multiple Output) control strategy. The linear model predictive control (LMPC) and predictive functional control (PFC) are the proposed advanced control algorithms to be tested.

The PFC technique was developed by Richalet [20] and has not been applied in many works in the available literature. Some applications can be found for the chemical industry [21], insulin dosage for a diabetes patient [22], heat exchangers [23] and parallel robot control [24].On the other hand, numerous studies have applied different LMPC approaches in fuel cell systems obtaining significant improvements in transient response and disturbance rejection [25–28]. Many researchers presented the controllability analysis with steady state information and the design of control structures for the BPS [29,30]. García et al. presented in Ref. [31] an ethanol steam reformer dynamic model based on energy and mass balances but without the purification unit, and designed a decentralized 2 × 2 structure. They conclude that more complex control structures would be required to exploit the coupled multivariable character of the system. Recio Garrido et al. proposed in Ref. [32] three optimization-based control configurations, a LMPC, a linear quadratic regulator with output error integral action and a cascade control combining the two previous configurations. These structures are applied in an isothermal model of a complete ethanol steam reformer and compared with a decentralized PI. However, none of the referred works designs the control structure and analyzes the dynamic behavior for the highly integrated process BPS + PEM-FC.

The paper is structured as follows: the next section presents a brief description of the bioethanol processor system. Section 3 presents the design and implementation of the proposed soft sensors. Section 4 presents an introduction to the model predictive control approaches, including the control objectives and tuning process. Section 5 presents the simulation results, including an analysis and comparison of the dynamic behavior and the operation costs of the proposed control structures. Finally, in Section 6 the conclusions are exposed.

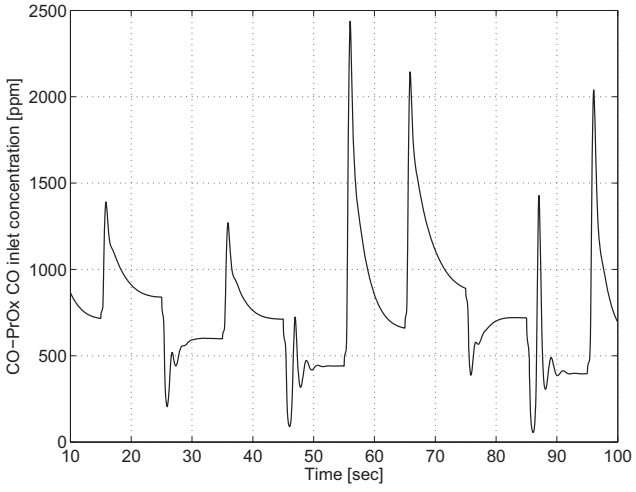

Fig. 4 – SS1 Training data – Output profile: CO-PrOx CO inlet concentration ($\widehat{y_9}$).

2. System description

A simplify scheme of the BPS with PEM-FC is displayed in Fig. 17(a). The main reactor, where most of the conversion of ethanol to H_2 is made, is the ESR. The CO concentration in the output stream is above PEM-FC accepted levels, so a cleaning

Table 3 – Soft Sensor 1 design parameters.

Parameter	Value
Hidden layers transfer function	'tansig'
Output layer transfer function	'purelin'
Training algorithm	Leverberg–Marquardt ('trainlm')
Performance function	'msereg'
Performance ratio (λ)	0.7
Maximum number of epochs to train	1000
Performance goal	0.00001
Learning rate	0.001
Learning rate increase	10
Learning rate decrease	0.1
Maximum learning rate	1e + 010

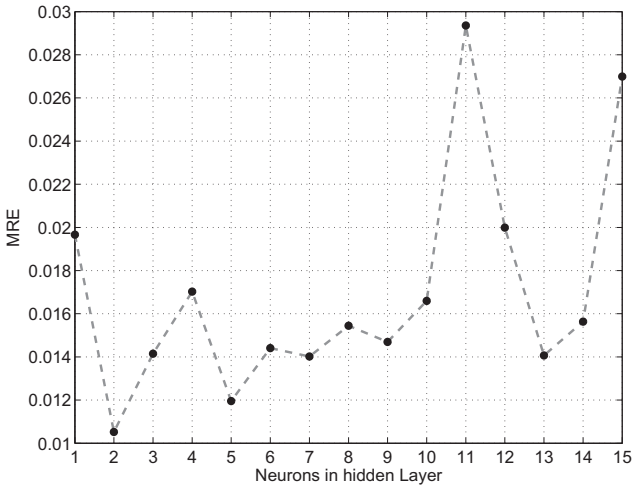

Fig. 5 – SS1 – Best MRE Value vs. number of neurons in hidden layer.

system must be included. Three reactors configure this stage; two Water Gas Shift, one of high temperature (HTS) and the other of low temperature (LTS), that favors the equilibrium of the reaction to higher conversion rates of CO; and a preferential oxidation of carbon monoxide (CO-PrOx) reactor, where oxidation of CO into CO_2 is made. Furthermore, the undesired oxidation of H_2 occurs, so the selection of a highly selective catalyst, the reactor design and the definition of the operation point are essential aspects. This operating point, which is critical in obtaining a good CO conversion, is defined by the catalyst temperature and the molar ratio O_2/CO. The pseudo dynamic model of this highly integrated system is presented in detail in Ref. [7]. The integration of the BPS and PEM-FC with an entire vehicle and the energy management strategy is made in Ref. [15]. To evaluate performance the Urban Dynamometer Driving Schedule (UDDS) is utilized. The resulting load profile demanded to the PEM-FC is plotted in Fig. 1.

3. Soft sensors

A soft sensor is a device where the output (predicted variable) can be modeled using other parameters or variables. Therefore, these devices consist in the association of an available process variable measurement (inputs), with an estimation algorithm (software) in order to infer unmeasurable variables (outputs). Artificial neural networks have been demonstrated to be a good option in industry to construct efficient models for estimating the temporal evolution of specific variables of the process. Hence, in the next subsection a brief review is given to explain the main steps to develop a soft sensor based on artificial neural network.

3.1. *Brief review of artificial neural networks*

Artificial neural networks are widely accepted as a technology to deal with complex and ill-defined problems, mainly because: they can learn from examples, are fault tolerant in the sense that they are able to handle noisy and incomplete data, are able to deal with nonlinear problems and, once trained, can perform prediction and generalization at high speed [13].

There are different types of neural networks. In function approximation and prediction application, one of the most commonly used neural network structure is the feedforward [33,34]. Neural networks consist of multiple layers of neurons, that apply nonlinear transfer functions between inputs and outputs. These characteristic allows them to learn and duplicate nonlinear relationships among variables. One of the first and most important steps in the developing of an ANN model is the definition of input and output variables and data preparation [35]. Output variable is obvious because it is the predicted, but input variables definition requires a deep knowledge of the process. If the considered variables have different units, it is very useful to pre-process all the data. In this paper a pre-processing step by normalization to zero mean and unit variance is proposed.

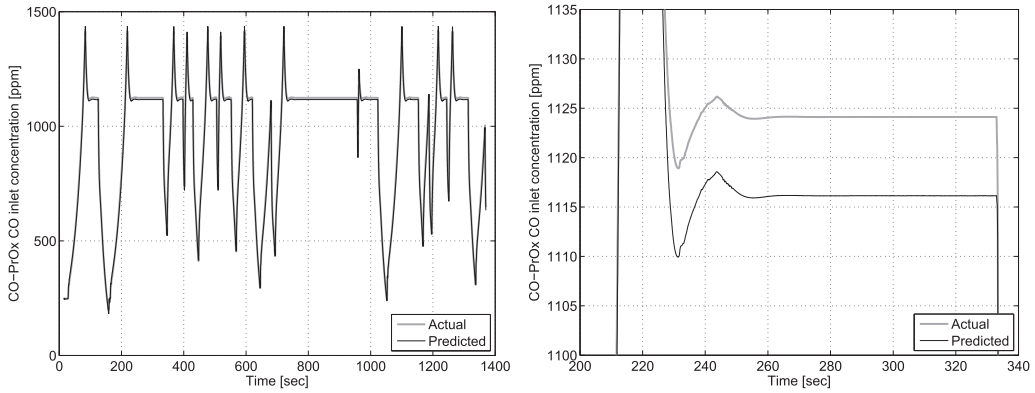

(a) CO-PrOx CO inlet prediction vs. Actual value

(b) Prediction detail

Fig. 6 – SS1 – Single hidden layer network prediction.

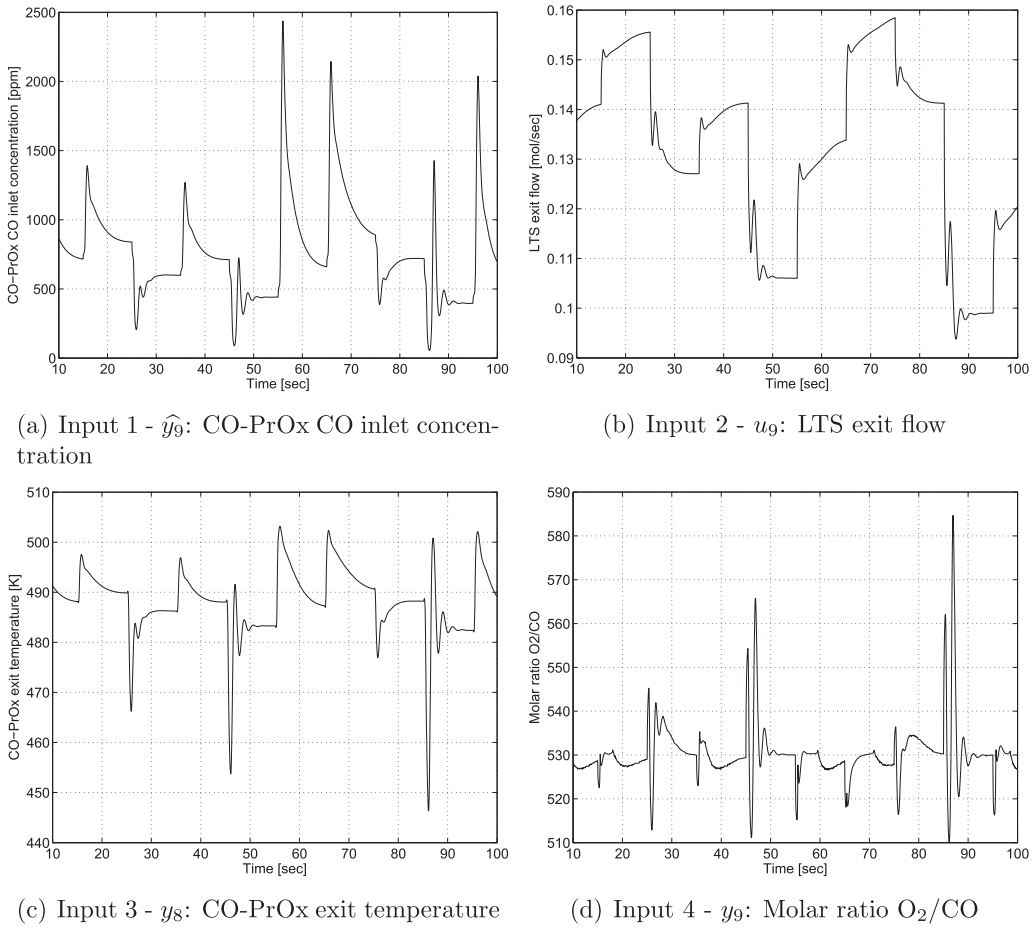

(a) Input 1 - $\widehat{y_9}$: CO-PrOx CO inlet concentration

(b) Input 2 - u_9: LTS exit flow

(c) Input 3 - y_8: CO-PrOx exit temperature

(d) Input 4 - y_9: Molar ratio O_2/CO

Fig. 7 – SS2 Training data – Input profiles.

3.1.1. *ANNs training, topology selection and validation*

Once the ANN model architecture is defined, inputs and outputs established and data collected, the network is then trained to recognize the relationships between input and output variables. For this purpose, the back-propagation algorithm with the Marquardt–Levenberg modification is used [36]. This is an iterative process where the weights associated with each connection are self-adjusting. The adjustment of the weights stops when an optimum value is obtained by maximizing or minimizing a performance function.

A typical problem that occurs during ANN training is called overfitting. It means that the network has memorized the training examples, but it has not learned to generalize. To avoid this drawback, the regularization method proposed by

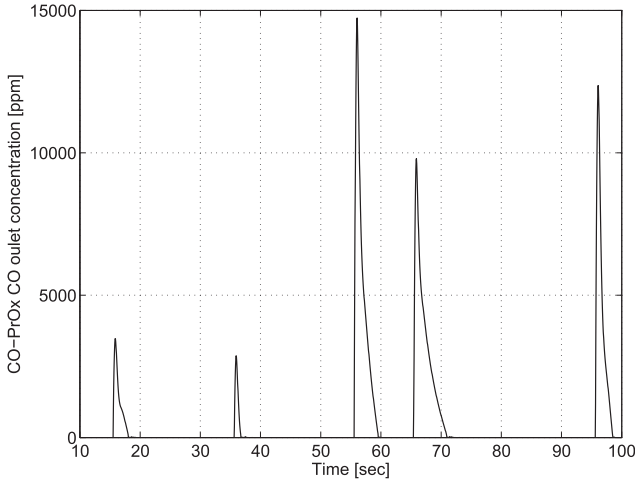

Fig. 8 – SS2 Training data – Output profile: CO-PrOx CO outlet concentration (y_{11}).

Table 4 – Soft sensor 2 design parameters.

Parameter	Value
Hidden layers transfer function	'tansig', 'poslin'
Output layer transfer function	'purelin'
Training algorithm	Leverberg–Marquardt ('trainlm')
Performance function	'msereg'
Performance ratio (λ)	0.8
Maximum number of epochs to train	1000
Performance goal	0.00001
Learning rate	0.001
Learning rate increase	10
Learning rate decrease	0.1
Maximum learning rate	1e + 010

Tikhonov [37] and implemented in the MatLab Neural Network Toolbox is applied [38]. The performance function results:

$$msereg = \lambda mse + (1-\lambda)msw = \lambda\frac{1}{N}\sum_{i=1}^{N}(e_i)^2 + (1-\lambda)\frac{1}{n}\sum_{j=1}^{n}(w_j)^2 \quad (1)$$

where N is the total training samples, t_i are the target samples and a_i the network outputs, λ is the performance ratio and w_j are the weights. With this modification on the performance function, the network response is forced to be smoother, and the overfitting is less likely. The performance ratio value is adjusted by trial and error.

One of the most critical decision in the design process of a feedforward Neural Network is choosing the number of hidden layers and the number of neurons in each one. Unfortunately there is no universal method to determine the optimum network topology. A possibility can be train different topologies and select the one with best validation performance. The validation is the process where networks are tested in order to judge its performance and to determine whether the predicted results confirm with the actual results. Typically, a performance index is calculated from actual and predicted variables for comparison purposes. Mean Relative Error (MRE), Root Mean Squared Error (RMSE) and FIT coefficient are mostly used.

$$\mathrm{MRE} = \frac{1}{n}\sum_{i=1}^{n}\frac{\left|\widehat{y_i} - y_i\right|}{|y_i|} \quad (2)$$

Table 5 – Soft sensor 2 – validation results.

n_1	n_2	RMSE [ppm]
1	15	3.474
1	3	3.477
1	7	3.490
1	11	3.499
1	10	3.547

$$\mathrm{RMSE} = \sqrt{\frac{1}{n}\sum_{i=1}^{n}\left(\widehat{y_i} - y_i\right)^2} \quad (3)$$

$$\mathrm{FIT} = \left(1 - \frac{\left\|\widehat{y_i} - y_i\right\|}{\left\|\widehat{y_i} - \overline{y}\right\|}\right) \times 100\% \quad (4)$$

where $\hat{y}$ is the vector of n predictions, y is the vector of n real values and $\overline{y}$ is the mean value of y.

3.2. Soft sensor design

The data set used for training the soft sensors is obtained by simulation of the rigorous model when the disturbance profile presented in Fig. 2 is applied. As it can be seen in the figure, the operative range of the PEM-FC is almost fully covered. Then, the most representative measurements for each predicted variables are used as inputs of the ANNs. Tables 1 and 2 indicates the inputs and predicted variables of Soft Sensor 1 (SS1) and Soft Sensor 2 (SS2). For validation purpose is used the disturbance profile of Fig. 1. For design, training and validation purpose, the MatLab Neural Network Toolbox is applied.

3.2.1. Soft sensor 1

Soft sensor 1 is in charge of the prediction of the CO-PrOx CO inlet concentration. Following the methodology stated in section 3.2, the LTS exit temperature (y7) and flow (u9) are the chosen input variables. The training data profiles are showed in Figs. 3 and 4. The data is preprocessed as is stated in section 3.1.1. The design parameters are shown in Table 3. Then, the number of neurons in the hidden layer must be selected. The different topologies resulting from varying the number of neurons from $n = 1$ to $n = 15$ are validated and the MRE index is calculated. This is a relative criteria, so the error is equally weighted throughout the entire range. As can be seen in Fig. 5, the best result is obtained for a network with 2 neurons in the hidden layer, resulting a MRE value of 0.010524 and a FIT of 96.359%. In Fig. 6 the dynamic response is shown. A steady state error of around 10 ppm is observed in Fig. 6(b). This means an acceptable performance.

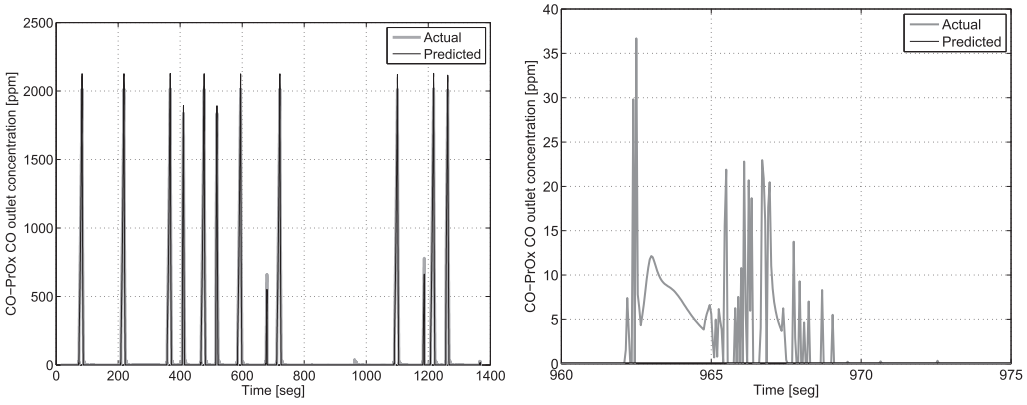

(a) CO-PrOx CO outlet prediction vs. Actual value

(b) Prediction detail

Fig. 9 – SS2 – 2 hidden layers network prediction.

Table 6 – Variables in the BPS + FC process.

Measured		Manipulated		Disturbances	
y_1	ESR exit temperature	u_1	Water to ESR inlet	d_1	Ethanol purity
y_2	Jacket exit gases temperature	u_2	Exchanged heat Q	d_2	Stack current
y_3	Burner exit temperature	u_3	Ethanol to Burner		
y_4	Burner entering molar flow	u_4	Oxygen to Burner		
y_5	Molar ratio H_2O/Ethanol	u_5	Oxygen to CO-PrOx		
y_6	HTS exit temperature	u_6	CM voltage		
y_7	LTS exit temperature	u_7	ESR exit flow (*)		
y_8	CO-PrOx exit temperature	u_8	HTS exit flow (*)		
y_9	Molar ratio O_2/CO	u_9	LTS exit flow (*)		
y_{10}	Burner exit molar flow	u_{10}	CO-PrOx exit flow (*)		
y_{11}	CO-PrOx CO outlet concentration	u_{11}	Bio-ethanol flow (*)		
y_{12}	Net Power				
y_{13}	Oxygen excess				
y_{14}	Stack voltage				
y_{15}	ESR pressure (*)				
y_{16}	HTS pressure (*)				
y_{17}	LTS pressure (*)				
y_{18}	CO-PrOx pressure (*)				
y_{19}	H_2 production rate (*)				

3.2.2. *Soft sensor 2*

Soft Sensor 2 predicts the CO-PrOx CO outlet concentration. Four variables are selected like inputs of the network: CO-PrOx CO inlet concentration ($\widehat{y_9}$), LTS exit flow (u_9), CO-PrOx exit temperature (y_8), Molar ratio O_2/CO (y_9), while CO-PrOx CO outlet concentration (y_{11}) is the predicted variable. Training data profiles are showed in Figs. 7 and 8. The same network architecture, training algorithm and performance function applied at SS1 is used here. The design parameters are shown in Table 4. In this case the single hidden layer network topology did not obtain acceptable results, hence only the ones with 2 hidden layers are presented. The output variable can only assume positive values. Due to this feature a linear transfer function with a saturation in zero is proposed in the second hidden layer, instead of a the classical sigmoid function.

Since this sensor is proposed mainly for monitoring purpose, the prime goal is to detect CO concentration traces above 10 ppm. Therefore, the validation criteria must assure a good performance in low range. The number of neurons in hidden layer 1 (n_1) and hidden layer 2 (n_2) are varied from 1 to 15 and the selection is made by an absolute index value, like RMSE, evaluated below a threshold of 100 ppm. The topologies with best performances are listed in Table 5. The network with $n_1 = 1$ and $n_2 = 15$ has the lower RMSE value, however a network with 3 neurons in the second layer reaches very similar values. As is said in section 3.1.1, the overfitting is a recurrent issue in ANN training, so the network with less number of neurons ($n_1 = 1$, $n_2 = 3$) is selected. It presents a RMSE value of 3.477 ppm below 100 ppm and a FIT of 71.25% calculated over the entire range. The prediction profile is shown in Fig. 9. A general good performance is seen, where most of the variable peaks above the critical value of 10 ppm are detected. Along the entire validation profile only a small amount of values above 10 ppm are not detected, and are presented in Fig. 9(b).

4. Control strategies

In this section the main control objectives of the system are listed. Furthermore, based on the decentralized control structure presented in Refs. [15], two advanced control strategies are proposed to maintain the CO levels within the desired range and to improve general dynamic behavior. The stack current profile presented in section 2 is used. This profile provides a great challenge to control structures.

4.1. *Decentralized PI*

The main control objectives of the BPS are:

- Maintain adequate H_2 levels on the anode of the PEM-FC, because starvation can cause permanent damage and overfeeding will lead to hydrogen waste.

Table 7 – RGA for the BPS + FC process.

	u_1	u_2	u_3	u_4	u_5	u_6
y_1	0.0001	**0.9908**	0.0074	0.0014	0.0004	0.0000
y_3	0.0242	0.0012	**0.8882**	0.0844	0.0020	0.0000
y_8	0.3953	0.0011	0.0143	0.0108	**0.5796**	−0.0011
y_9	**0.5776**	0.0005	0.0004	0.0027	0.4187	0.0000
y_{10}	0.0031	0.0064	0.0897	**0.9008**	0.0000	0.0000
y_{13}	−0.0003	0.0000	0.0000	−0.0000	−0.0007	**1.0011**

Bold values represent RGA values of the selected control loops.

Table 8 – Operating point for internal model.

Variable	Description	Nominal point	Unit
d_2	Stack current	200.00	[A]
u_1	Water to ESR inlet	0.06001	[mole/s]
u_5	Oxygen to CO-PrOx	0.00143	[mole/s]
y_8	CO-PrOx temperature	530.00	[K]
y_9	Molar ratio O_2/CO	2.00	

- The CO concentration in the PEM-FC anode stream must be kept under 10 ppm.
- Keeping the temperatures of the reactors set and PEM-FC at their operational range.
- Maintain system efficiency.

The set of available variables in the BPS are listed in Table 6, and with (*) are indicated the stabilizing control loops. As can be seen, six manipulated variables (MVs) are available (u_1–u_6). The plant wide control design methodology applied in Ref. [15] proposes the optimal controlled variables (CVs) selection and based on the well-known RGA approach [39], a decentralized control structure is implemented. The RGA allows to define the input–output pairing by using steady-state information. The values are showed in Table 7, and the six control loops are: 1, y_9–u_1; 2, y_1–u_2; 3, y_3–u_3; 4, y_{10}–u_4; 5, y_8–u_5 and 6, y_{13}–u_6. These are implemented via conventional SISO PI controllers and tuning based on internal model control (IMC) strategy. A detailed description of the methodology and tuning process and values can be seen in Refs. [15,40]. The resulting control structure is shown in Fig. 17(b). A good dynamic performance is achieved with the proposed policy. However, through the implementation of the soft sensor 2, large transient values can be seen in the CO-PrOx CO outlet concentration (y_{11}). An improvement on disturbance rejection in loop 5 and mainly in loop 1 could avoid the rise of y_{11} beyond the required limits. In the next section, model predictive control is applied in order to satisfy this request.

4.2. *Model predictive control*

Model predictive control are a family of algorithms that utilize an explicit process model to predict the future response of a plant. Then, the optimization of an open-loop performance objective over a future time horizon is solved resulting in a sequence of manipulated variable movements. At each control interval only the first item in the optimal sequence is applied and the rest is discarded. The entire calculation is repeated at subsequent control intervals with the process measurements used to update the optimization problem. Different control companies implement MPC by adopting specific characteristics to attend a wide range of real problems in industry. In this section two different technologies are evaluated to improve the achievable performance of a conventional decentralized PI control, both of them are very well known in chemical industries and linear based strategies. Hence, the most popular linear model predictive control and the predictive functional control are considered. A thorough review of different industrial model predictive control technology is presented in Ref. [41]. However, there is no enough information about available criteria to decide the MPC implementation. One natural rule is consider that if the interaction degree is very important to deteriorate the dynamic performance, is convenient to evaluate the real contribution to be expected from this kind of advanced control. In this context, the following subsection describes the characteristics of the Relative Gain Matrix analysis to determine the interaction degree related to specific pairing between input–output variables.

4.2.1. *Interaction relative gain array analysis*

The study of the RGA provides two important elements: a recommendation of an effective pairing of controlled and manipulated variables, and a measure of process interactions. In the implementation of a decentralized structure only the first item is considered when the pairing is defined. However, the degree of interaction between control loops may degrade the performance of controlled variables. A RGA matrix with all

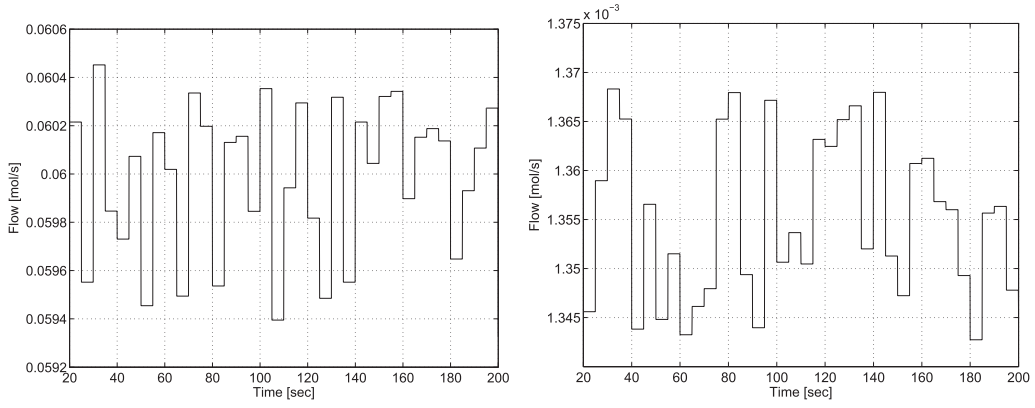

(a) ESR water inlet flow (b) Oxygen to CO-PrOx flow

Fig. 10 – Manipulated variables identification data.

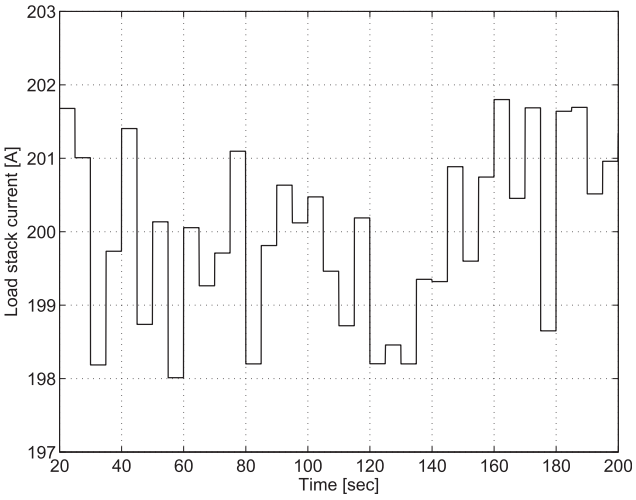

Fig. 11 – Disturbance identification data – Load stack current.

ones in the diagonal elements (λ_{ij} with $i = j$) is always desirable, because it means that system loops are not interacted and a decentralized control structure with PI loops could be implemented. Moreover, when the elements λ_{ij} have values near 0.5, the loops could be considered highly interacted [42,43]. As can be seen in the case study RGA matrix presented in Table 7, λ_{31}, λ_{41}, λ_{35} and λ_{45} has all values near 0.5 so loop 1 and loop 5 present interaction effects. The resulting 2 × 2 subsystem with CVs (y_8, y_9) and MVs (u_1, u_5) is therefore a good multivariable control strategy candidate.

4.2.2. *Linear model predictive control*

Generally, the LMPC is formulated in the state space form. The system to be controlled is described by a linear discrete time model.

$$\begin{aligned} x(k+1) &= \hat{A}x(k) + \hat{B}(u_t(k)) \\ \hat{y}(k) &= \hat{C}x(k) \end{aligned} \tag{5}$$

where $u_t = [u, d]^T$ is the model input vector with the manipulated input vector u and the measured disturbance vector d. x is the state space vector and $\hat{y}$ is the output vector [44]. The model defined by $u_t = [u_1, u_5, d_2]^T$ and $\hat{y} = [y_8, y_9]^T$ is identified around the operating point shown in Table 8. Inputs are simultaneously perturbed with random steps from their nominal values. Then, adopting a sampling time $T_s = 0.05$ s, 4000 samples are collected. Values are normalized to zero mean and unit variance, and using the *n4sid* method from the System Identification Toolbox of MATLAB, and a 10th order model is obtained. Identification data are shown in Figs. 10 and 11, and results in Fig. 12. Having the internal model, the future control moves vector $\Delta u(k)$ is the solution of a quadratic optimization problem of the form:

$$\begin{aligned} min_{\Delta u(k)} J = &\sum_{i=1}^{P} e(k+i)^t Q e(k+i) + \sum_{i=1}^{M} u(k+i)^t S u(k+i) \\ &+ \Delta u(k+i-1)^t R \Delta u(k+i-1) \end{aligned} \tag{6}$$

subject to

$$\hat{y}^{min} \le \hat{y}(k+i) \le \hat{y}^{max} \tag{7}$$

$$u^{min} \le u(k+i) \le u^{max} \tag{8}$$

$$\Delta u^{min} \le \Delta u(k+i) \le \Delta u^{max} \tag{9}$$

The value $e(k+i)$ is the predicted error at time $k+i$,

$$e(k+i) = y_{sp}(k+i) - \hat{y}(k+i) \tag{10}$$

where y_{sp} is the output set-point. P denotes the length of the prediction horizon, and M denotes the length of the control horizon. The matrices Q, R and S are the penalty matrices of outputs, inputs and rate of change of inputs, and are assumed to be symmetric positive definite. The tuning of the different parameters of LMPC is still an open issue. An interesting review of several tuning methods can be found in Ref. [45]. In this work, the tuning approach proposed by Shridhar and Cooper in Ref. [46] is applied. The values of different LMPC parameters are shown in Table 9. Constraints

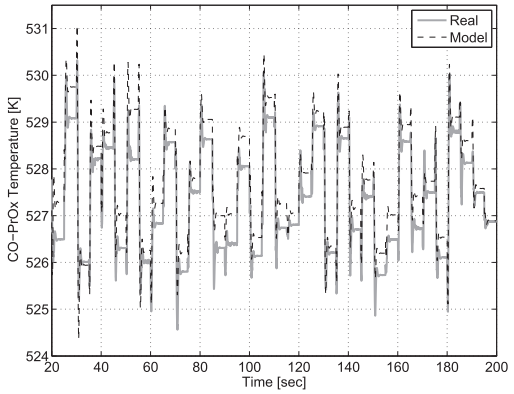

(a) CO-PrOx exit temperature (y_8) - Model Output FIT = 77.04%

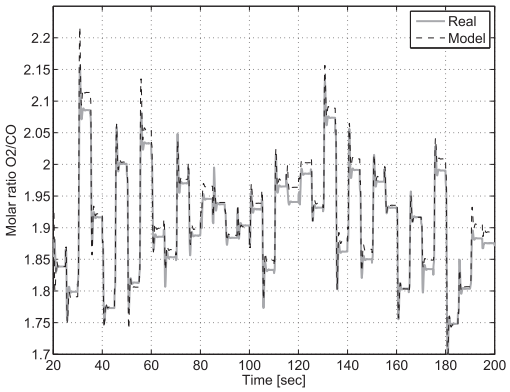

(b) Molar ratio O_2/CO (y_9) - Model Output FIT = 87.54%

Fig. 12 – Controlled variables model fitting.

Table 9 – LMPC tunning parameters.

Symbol	Description	Value
P	Prediction horizon (samples)	100
M	Control horizon (samples)	5
q_{y8}	Output weight (y_8)	1
q_{y9}	Output weight (y_9)	10
s_{u1}	Input weight (u_1)	0
s_{u5}	Input weight (u_5)	0
r_{u1}	Input rate weight (Δu_1)	8.7
r_{u5}	Input rate weight (Δu_5)	2.5

Table 10 – PFC tunning parameters.

Symbol	Description	Value	Unit
$Trbf_H$	Closed loop time response – Hight	100	[sec]
$Trbf_L$	Closed loop time response – Low	2	[sec]
Δ	Transition zone	0.2	[%]
H	Number of coincidence points	1	
H_1	Initial coincidence horizon	0.4	[sec]
H_2	Final coincidence horizon	0.4	[sec]
T_s	Sampling time	0.05	[sec]
K_{mi}	Model Gain	265.6	
T_{mi}	Model time constant	0.65112	[sec]
θ_{mi}	Model time delay	0	[sec]
K_{di}	Disturbance Gain	−0.07431	
T_{di}	Disturbance time constant	0.60892	[sec]
θ_{di}	Disturbance time delay	0	[sec]

are established only in manipulated variables, in order to maintain them positive. Finally, the resulting control scheme is shown in Fig. 17(c) and implemented with the MPC toolbox of MATLAB.

4.2.3. *Predictive functional control*

The PFC option is recommended to be considered when the plant wide control works well but one loop presents troubles which affect the overall behavior. The H_2 production plant analyzed here seems to indicate this kind of problem around the CO-PrOx reactor. In particular, the most relaxed version of PFC was specially proposed to be used in reactors and it was presented as PCR which means Predictive Control of Reactors. The main PFC controller elements are: internal process dynamic model, a reference trajectory $y_r(n)$ that can be interpreted as the desired closed loop behavior, a self-compensation of the predicted error and a specific structure for the manipulated variable. Based on the prediction of the internal model, the future error with respect to the desired trajectory is calculated over the coincidence horizon (H_1, H_2). The actual measured data is used in the compensation of the plant-model mismatch. The model prediction could be improved using extrapolation to estimate the future error at the coincidence horizon. An important feature of PFC is that feed-forward and feedback control actions can be jointly designed and constraints are taken into account in a very natural way. Calling the inputs of the manipulated variable $u(n)$ and the perturbation $d(n)$, the first order model response at the coincidence point $(n + H)$ becomes:

$$y_m(n+H) = \alpha_m^H x_{mi}(n) + \alpha_d^H x_{md}(n) + \sum_{j=0}^{H-1} \alpha_m^{H-1-j} K_{mi}(1-\alpha_m)u(j+n) + \sum_{j=0}^{H-1} \alpha_d^{H-1-j} K_{di}(1-\alpha_d)d(j+n) \tag{11}$$

$$u(n) = K_0\hat{\varepsilon}(n) + K_1 y_{mi}(n) + \ldots + K_2 y_{md}(n) + K_3 d(n) + K_4 y_m(n) \tag{12}$$

$$K_0 = \frac{(1-\lambda^H)}{K_{mi}(1-\alpha_m^H)} \tag{13}$$

$$K_1 = \frac{-\alpha_m^H}{K_{mi}(1-\alpha_m^H)} \tag{14}$$

$$K_2 = \frac{-\alpha_d^H}{K_{mi}(1-\alpha_m^H)} \tag{15}$$

$$K_3 = \frac{-K_{di}(1-\alpha_d^H)}{K_{mi}(1-\alpha_m^H)} \tag{16}$$

$$K_4 = \frac{1}{K_{mi}(1-\alpha_m^H)} \tag{17}$$

When only one coincidence point is used PFC becomes on PCR and presents the important advantage of requiring less computation time. In addition it results more intuitive for the users. It was demonstrated that the controller transfer function has an implicit integrator which guarantees zero tracking error for step inputs. The name "functional" is related to the use of base functions for defining the manipulated variable. Typically these functions are steps $B_1(i) = 1$; ramps $B_2(i) = i$ or parabolas $B_3(i) = i^2$. The choice of the basis functions defines the input profile and can assure a predetermined behavior. The reference trajectory, which is the path to the future set point, is resetted at every instant and is given by:

$$C(n+j) - y_r(n+j) = \lambda^j\Big(C(n) - y_p(n)\Big), 0 \le j \le H \tag{18}$$

$$\lambda = e^{\frac{-3T_s}{CLTR}} \tag{19}$$

where $C(n)$ is the set-point, $y_p(n)$ the real process output and λ is a parameter that represents the exponential convergence of the algorithm, and thus fixes the closed-loop behavior. T_s is the sampling time and was considered as 0.05 s.

The parameters to be tuned for the PFC are: number of coincidence points (H), closed loop time response (CLTR) of the reference trajectory, the control zone considered so that CLTR moves linearly between two extremes values recognized as *CLTR_L* (low) and *CLTR_H* (high), the *transition zone* [%] that set the allowed zone for the controlled variable expressed as ±*Delta* [%] with respect to the set point value and constraints to the manipulated variable are also included by fixing maximum (U_{max}), minimum (U_{min}) and variations for it [$(dU/dt)_{max}$]. For more details about the implementation of PFC, the reader should see Ref. [47]. As it was said before, the control loop with the greatest influence

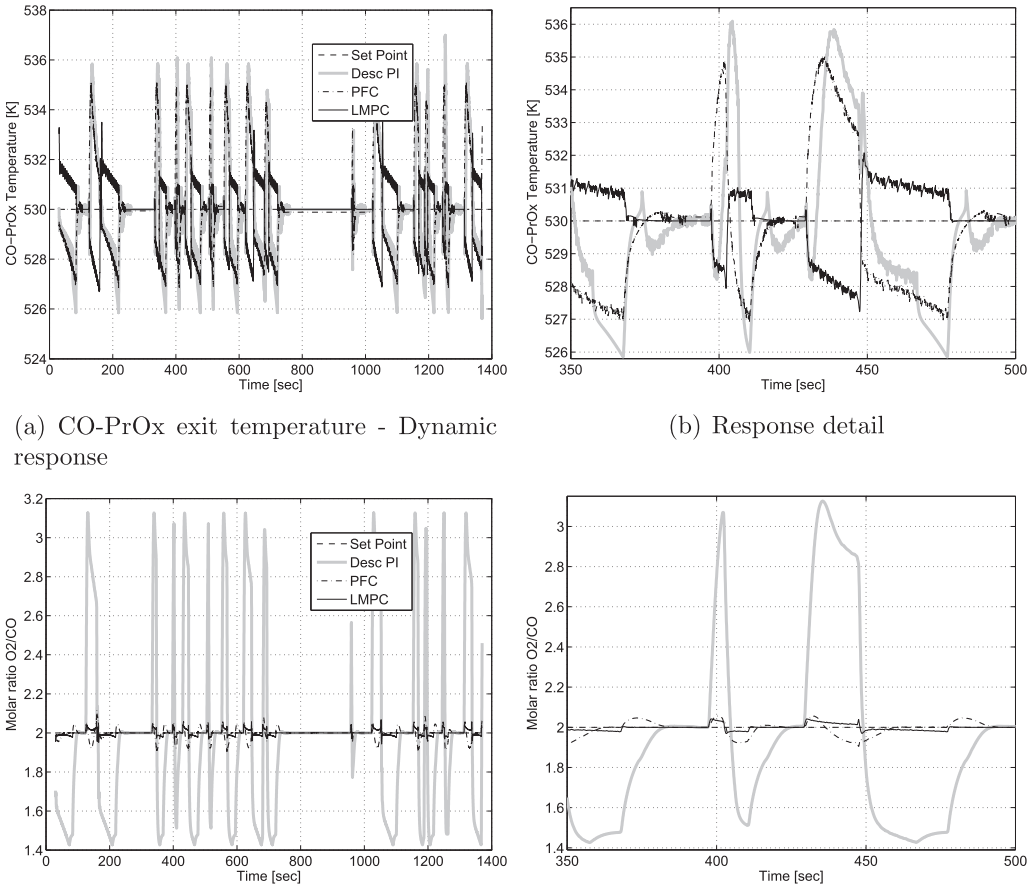

(a) CO-PrOx exit temperature - Dynamic response

(b) Response detail

(c) Molar ratio O_2/CO - Dynamic response

(d) Response detail

Fig. 13 – Controlled variables (CVs) dynamic response for proposed control structures.

to this variable is loop 5. Therefore, the implementation of the PFC algorithm instead of PI based loop is tested. The resulting control configuration is shown in Fig. 17(d). For the development of the first order transfer functions used, a step test is applied to the plant and *pem* function of System Identification Toolbox of MATLAB is used. The detailed parameter values are shown in Table 10.

5. Simulations results

In this section dynamic simulation results and index performance values are presented. The control strategies developed are tested for disturbance rejection and contrasted with the decentralized PI-IMC policy. It can be seen in Figs. 13 and 14 the controlled variables response, while manipulated variables profile are shown in Fig. 16. In Fig. 15 the dynamic response of the CO-PrOx CO outlet concentration is shown. Finally, the performance index values of the main outputs and the control energy of inputs are presented and compared. For CVs performance evaluation the integral absolute error (IAE) is used. Then, in order to compare between control structures, the error improvement percent (EIP) is applied.

$$\mathrm{IAE} = \sum_{k} |r(k) - y(k)| \tag{20}$$

where $r(k)$ represent set point and $y(k)$ the controlled variable.

$$\mathrm{EIP} = \frac{IAE^{base} - IAE^{new}}{IAE^{base}} \times 100\% \tag{21}$$

where *base* refers to the decentralized control strategy proposed as reference, and *new* denotes the MPC designs developed in this work. The EIP index can be obtained for each CV. The *new* control strategy is better than the *base* one if the EIP index is positive.

Simulation results of y_8 are shown in Fig. 13(a). As can be seen, the LMPC structure presents better dynamic response than the other strategies, with overshoots of ±2.5 K, while PFC and PI-IMC presents ±5 K and ±6.3 K respectively. This improvement can also be seen in performance index values showed in Table 11, where PFC presents an EIP of 0.59% with respect to PI-IMC, while LMPC shows an EIP of 44.21%.

In Fig. 13(c) the dynamic responses of y_9 are shown. This variable shows one of the most significant improvements of the proposed control strategies with respect to the PI-IMC. A reduction in overshoots in the order of 95% is obtained with either model predictive approaches. PI-IMC presents overshoots above set-point of 1.2 while PFC shows values of 0.05

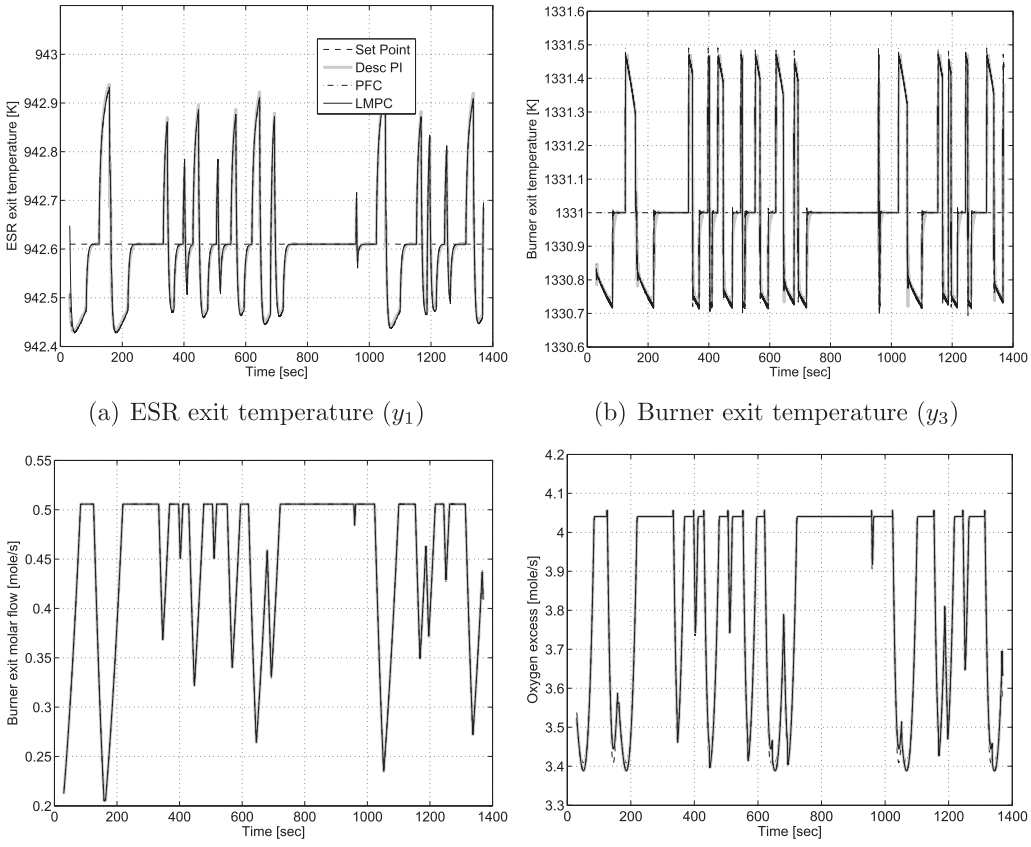

(a) ESR exit temperature (y_1) (b) Burner exit temperature (y_3)

(c) Burner exit molar flow (y_{10}) (d) Oxygen excess (y_{13})

Fig. 14 – Controlled variables (CVs) dynamic response for PI-IMC loops.

and in LMPC they are limited to 0.03. For overshoots below set-point, PI-IMC shows values of 0.6 while PFC 0.1 and LMPC 0.03. This is a very important issue, since a significant reduction in O_2/CO ratio produces an increment in CO-PrOx CO outlet concentration. For the same variable the performance index values show a reduction in the PFC IAE value of 94.86% (EIP) with respect to the PI-IMC, while the LMPC strategy presents a reduction of 97.17%. Furthermore, the rest of the controlled variables remains unchanged as can be seen in Fig. 14 and in EIP values.

Table 12 shows the control energy values of manipulated variables for each control approach. These are a measure of the operational costs. As can be seen, there are no significant differences between structures. If u_1 values are analyzed, it can be seen an increment in control energy, regarding to PI-IMC, of 0.84% in the case of LMPC and a 0.91% with PFC. Moreover, small differences can be seen in the dynamic behavior of the manipulated variables u_1 and u_5 showed in Fig. 16(b) and (d), but these are enough to produce the improvements showed before.

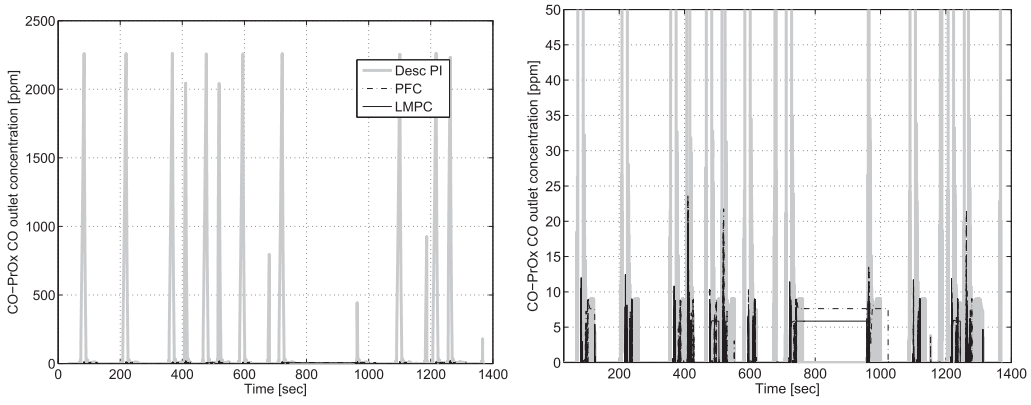

(a) CO-PrOx CO outlet concentration (y_{11}) (b) Response detail below 50 ppm

Fig. 15 – CO-PrOx CO outlet concentration response for proposed control structures.

Table 11 – Dynamic performance of CVs – UDDS disturbance profile.

CV	Description	PI-IMC IAE	LMPC		PFC	
			IAE	EIP_{PI} [%]	IAE	EIP_{PI} [%]
y_1	ESR exit temperature	1999.3	2034.7	−1.769	2050	−2.537
y_3	Burner exit temperature	3665.7	3740.8	−2.0475	3805.1	−3.8037
y_8	CO-PrOx exit temperature	32425	18088	**44.216**	32232	**0.5964**
y_9	Molar ratio O_2/CO	7967	225.48	**97.17**	409.47	**94.86**
y_{10}	Burner exit molar flow	22.241	21.148	4.915	21.302	4.2229
y_{11}	CO-PrOx CO outlet concentration	1.847×10^6	1.6911×10^4	**99.085**	2.3902×10^4	**98.706**
y_{12}	Net Power	240.86×10^6	240.86×10^6	0	240.86×10^6	0
y_{13}	Oxygen excess	509.64	509.64	0	509.64	0
y_{19}	H_2 production rate	4.5986×10^{-3}	4.6574×10^{-3}	−1.2776	4.7387×10^{-3}	−3.0465

Bold values are performance index values referred in "Simulation results" section.

Table 12 – Control energy – UDDS conditions.

MVs	Description	PI-IMC	LMPC	PFC
u_1	Water to ESR inlet	109.6318	110.5526	110.6228
u_2	Exchanged heat Q	36.3042	36.4473	36.4473
u_3	Ethanol to Burner	7.8160	7.8441	7.8441
u_4	Oxygen to Burner	1576.4	1572.0	1571.6
u_5	Oxygen to CO-PrOx	0.096683	0.097174	0.097003
u_6	CM voltage	9.8054×10^{11}	9.8054×10^{11}	9.8054×10^{11}
u_{11}	Bio-ethanol flow	9.1797	9.1531	9.1514

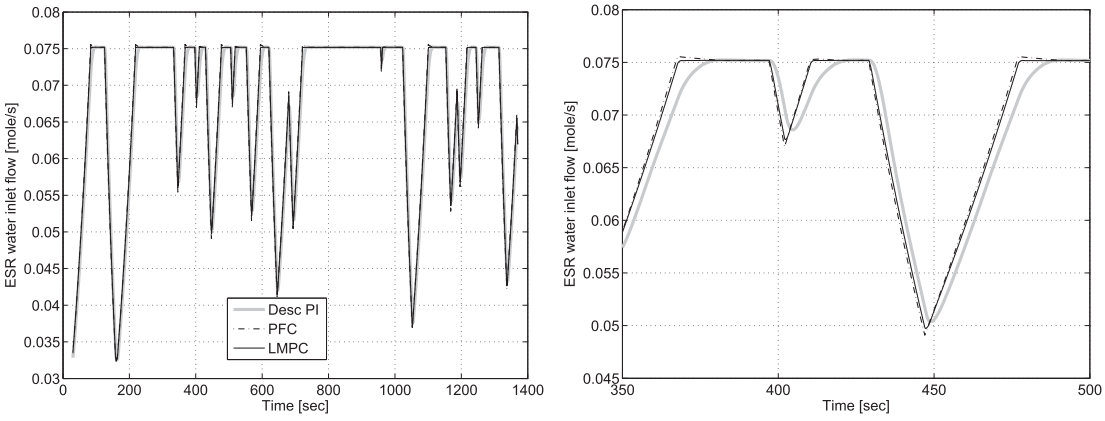

(a) ESR water inlet flow (u_1) (b) Response detail

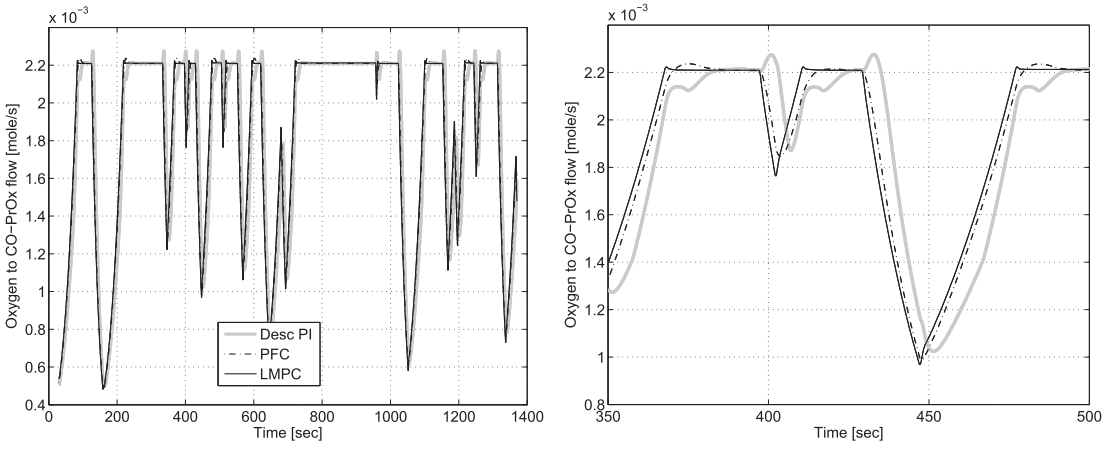

(c) Oxygen to CO-PrOx flow (u_5) (d) Response detail

Fig. 16 – Manipulated variables (MVs) dynamic response for proposed control structures.

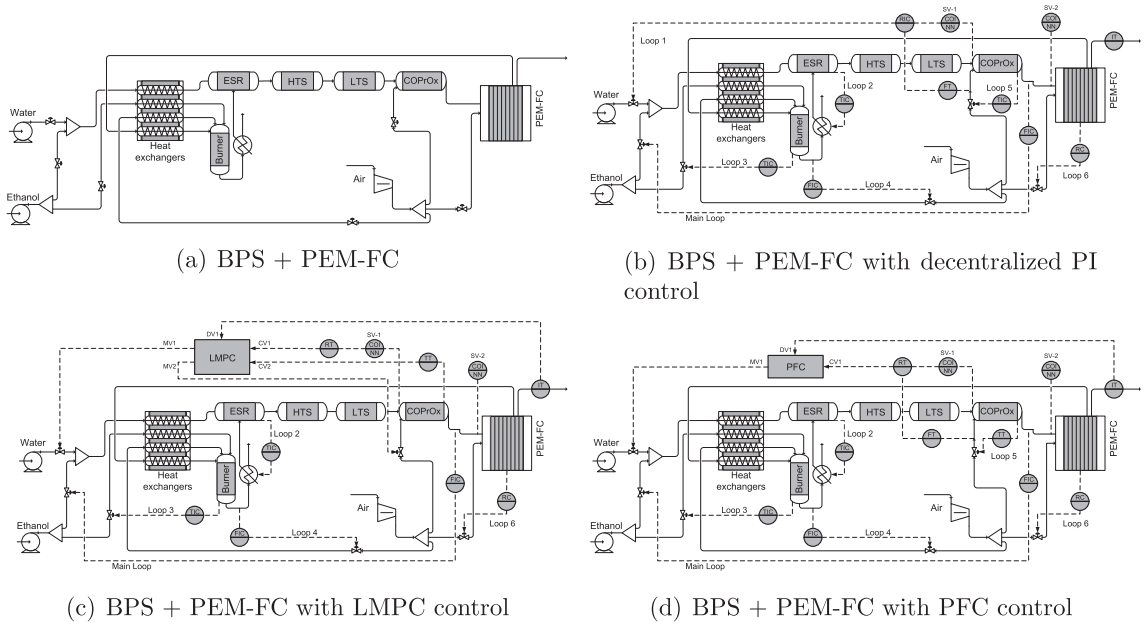

(a) BPS + PEM-FC

(b) BPS + PEM-FC with decentralized PI control

(c) BPS + PEM-FC with LMPC control

(d) BPS + PEM-FC with PFC control

Fig. 17 – BPS + PEM-FC Control structures.

LMPC and PFC strategies generate control movements more aggressive than PI-IMC, mainly because they can predict the influence of the measured disturbance in the controlled variable and produce a manipulated variable accordingly, instead of PI-IMC that begins to act once produced the effect on output. The possibility of interactions handling of the LMPC approach provides improvements with respect to PFC, but not really significant.

These important advances in dynamic behavior of CO-PrOx variables result in a significant improvement in CO-PrOx CO outlet concentration. In Fig. 15 can be seen a CO concentration satisfying the PEM quality requirement (<10 ppm) with both MPC approaches at almost all the tested range, except for short-time peaks of 20 ppm when PFC is used. For PI-IMC strategy peaks that reach the 2200 ppm during 30 s appear and must be taken into account in order to preserve the performance of the stack.

Finally, another important issue to analyze is the influence in system efficiency. It is directly affected by Net Power (y_{12}) and inversely by ethanol consumption (u_1, u_{11}). These variables remain the same for the PI-IMC and model predictive control schemes, so the efficiency does not seem affected.

6. Conclusions

This work proposes the implementation of model predictive control techniques in order to improve the disturbance rejection of a bioethanol processor system to satisfy the PEM-FC quality restriction in the hydrogen-rich stream. The study of the RGA matrix demonstrates that CO-PrOx is the most interacted zone of the system, therefore it represents a good candidate to be controlled with MPC. Significant improvements are obtained with both structures, LMPC and PFC, in regard to the decentralized PI control. The large number of tuning parameters involved on MPC techniques adds flexibility to the tuning procedure, but simultaneously, it makes proper tuning more difficult to be found. However, it is considered that PFC strategy is more intuitive than LMPC for selecting the parameters and can give reasonable results. Hence, PFC, or more specifically PCR, is the best candidate to be implemented in this plant. In addition, PCR demonstrated to be able of keeping the carbon monoxide concentration for feeding the fuel cell below 10 ppm almost for the entire disturbance profile. The use of virtual sensors for testing efficiently the carbon monoxide concentration was helpful to ensure safety conditions for the PEM operation. Therefore, the two soft sensors presented here represent an interesting option since this kind of commercial sensors are not easily available. In this context, the use of advanced control only for one problematic loop and the virtual sensor for checking on line a very important variable represent a real improvement to the existent plant wide control.

REFERENCES

[1] Thomas CS. Transportation options in a carbon-constrained world: hybrids, plug-in hybrids, biofuels, fuel cell electric vehicles, and battery electric vehicles. Int J Hydrogen Energy 2009;34(23):9279–96.

[2] Pukrushpan J. Modeling and control of fuel cell systems and fuel processors [Ph.D. thesis]. University of Michigan; 2003.

[3] Chrenko D, Gao F, Blunier B, Bouquain D, Miraoui A. Methanol fuel processor and {PEM} fuel cell modeling for mobile application. Int J Hydrogen Energy 2010;35(13):6863–71.

[4] Altieri M. Los impactos ecologicos de los sistemas de produccion de biocombustibles a base de monocultivos a gran escala en america, Agroecologa 4(0).

[5] Paganelli A, Gnazzo V, Acosta H, Lopez SL, Carrasco AE. Glyphosate-based herbicides produce teratogenic effects on

vertebrates by impairing retinoic acid signaling. Chem Res Toxicol 2010;23(10):1586–95.
[6] Garcia E, Laborde M. Hydrogen production by the steam reforming of ethanol: thermodynamic analysis. Int J Hydrogen Energy 1991;16(5):307–12.
[7] Nieto Degliuomini L, Biset S, Luppi P, Basualdo MS. A rigorous computational model for hydrogen production from bio-ethanol to feed a fuel cell stack. Int J Hydrogen Energy 2012;37(4):3108–29.
[8] Farrell C, Gardner C, Ternan M. Experimental and modelling studies of {CO} poisoning in {PEM} fuel cells. J Power Sources 2007;171(2):282–93.
[9] AS-MLC. Carbon monoxide sensor, appliedsensor. https://www.appliedsensor.com.
[10] Plus S. Carbon monoxide sensor, sensorstecnics, semiconductors, s.l, honeywell. http://www.honeywellanalytics.com/.
[11] Kirby KW, Chu AC, Fuller KC. Detection of low level carbon monoxide in hydrogen-rich gas streams. Sens Actuators B Chem 2003;95(13):224–31.
[12] Rallo R, Ferre-Gin J, Arenas A, Giralt F. Neural virtual sensor for the inferential prediction of product quality from process variables. Comput Chem Eng 2002;26(12):1735–54.
[13] Kalogirou SA. Artificial neural networks in renewable energy systems applications: a review. Renew Sustain Energy Rev 2001;5(4):373–401.
[14] Yap WK, Ho T, Karri V. Exhaust emissions control and engine parameters optimization using artificial neural network virtual sensors for a hydrogen-powered vehicle. Int J Hydrogen Energy 2012;37(10):8704–15.
[15] Nieto Degliuomini L, Zumoffen D, Basualdo M. Plant-wide control design for fuel processor system with pemfc. Int J Hydrogen Energy 2012;37(19):14801–11.
[16] Luppi P, Zumoffen D, Basualdo M. Decentralized plantwide control strategy for large-scale processes. case study: pulp mill benchmark problem. Comput Chem Eng 2013;52(0):272–85.
[17] Molina G, Zumoffen D, Basualdo M. A new systematic approach to find plantwide control structures. Comput Aided Chem Eng 2009;27:1599–604.
[18] Zumoffen D, Basualdo M. Optimal sensor location for chemical process accounting the best control configuration. Comput Aided Chem Eng 2009;27:1593–8.
[19] Molina G, Zumoffen D, Basualdo M. Plant-wide control strategy applied to the tennessee eastman process at two operating points. Comput Chem Eng 2011;35(10):2081–97.
[20] Richalet J. Pratique de la Commande Predictive. Paris-France: Editorial Hermes; 1993.
[21] Bouhenchir H, Cabassud M, Lann ML. Predictive functional control for the temperature control of a chemical batch reactor. Comput Chem Eng 2006;30(67):1141–54.
[22] Campetelli G, Zumoffen D, Basualdo M, Rigalli A. Testing PFC controller on a well validated in silico model of a type I diabetic patient. In: 9th international symposium on dynamics and control of process systems, Leuven, Belgium 2010.
[23] Abdelghani-Idrissi M, Arbaoui M, Estel L, Richalet J. Predictive functional control of a counter current heat exchanger using convexity property. Chem Eng Process Process Intensif 2001;40(5):449–57.
[24] Vivas A, Poignet P. Predictive functional control of a parallel robot. Control Eng Pract 2005;13(7):863–74.
[25] Arce A, del Real A, Bordons C, Ramirez D. Real-time implementation of a constrained mpc for efficient airflow control in a pem fuel cell. Ind Electron IEEE Trans 2010;57(6):1892–905.
[26] Feroldi D, Serra M, Riera J. Performance improvement of a {PEMFC} system controlling the cathode outlet air flow. J Power Sources 2007;169(1):205–12.
[27] Gruber J, Doll M, Bordons C. Design and experimental validation of a constrained {MPC} for the air feed of a fuel cell. Control Eng Pract 2009;17(8):874–85.
[28] Bao C, Ouyang M, Yi B. Modeling and control of air stream and hydrogen flow with recirculation in a {PEM} fuel cell system—II. Linear and adaptive nonlinear control. Int J Hydrogen Energy 2006;31(13):1897–913.
[29] Biset S, Degliuomini LN, Basualdo M, Garcia V, Serra M. Analysis of the control structures for an integrated ethanol processor for pem fuel cell systems. J Power Sources 2009;192(1):107–13.
[30] García VM, López E, Serra M, Llorca J, Riera J. Dynamic modeling and controllability analysis of an ethanol reformer for fuel cell application. Int J Hydrogen Energy 2009;35(18):9768–75. http://dx.doi.org/10.1016/j.ijhydene.2009.09.064.
[31] García VM, Serra M, Llorca J, Riera J. Design of linear controllers applied to an ethanol steam reformer for {PEM} fuel cell applications. Int J Hydrogen Energy 2013;38(18):7640–6.
[32] Recio-Garrido D, Ocampo-Martinez C, Serra-Prat M. Design of optimization-based controllers applied to an ethanol steam reformer for hydrogen production. Int J Hydrogen Energy 2012;37(15):11141–56.
[33] Ho T, Karri V, Lim D, Barret D. An investigation of engine performance parameters and artificial intelligent emission prediction of hydrogen powered car. Int J Hydrogen Energy 2008;33(14):3837–46.
[34] Zamaniyan A, Joda F, Behroozsarand A, Ebrahimi H. Application of artificial neural networks (ann) for modeling of industrial hydrogen plant. Int J Hydrogen Energy 2013;38(15):6289–97.
[35] Al-Alawi A, Al-Alawi SM, Islam SM. Predictive control of an integrated pv-diesel water and power supply system using an artificial neural network. Renew Energy 2007;32(8):1426–39.
[36] Hagan MT, Menhaj MB. Training feedforward networks with the Marquardt algorithm. IEEE Trans Neural Netw 1994;5(6):989–93.
[37] Tikhonov A. Solution of incorrectly formulated problems and the regularisation method. Sov Math Dokl 1963;4:10351038.
[38] MATLAB, version 7.10.0 (R2010a). Natick, Massachusetts: The MathWorks Inc.; 2010.
[39] Bristol E. On a new measure of interaction for multivariable process control. IEEE Trans Autom Control 1966;11(1):133–4.
[40] Rivera D. Una metodología para la identificacion integrada con el diseño de controladores IMC-PID. RIAI (Rev Iberoamericana de Autom e Inf Ind) 2007;4(4):5–18.
[41] Qin S, Badgwell T. A survey of industrial model predictive control technology. Control Eng Pract 2003;11(7):733–64.
[42] Seborg DE, Edgar TF, Mellichamp DA. Process dynamic and control. 2nd ed. New York, NY: Wiley; 2004.
[43] Skogestad S, Postlethwaite I. Multivariable feedback control. Analysis and design. John Wiley & Sons; 2005.
[44] Morari M, Lee JH. Model predictive control: past, present and future. Comput Chem Eng 1999;23(45):667–82.
[45] Garriga JL, Soroush M. Model predictive control tuning methods: a review. Ind Eng Chem Res 2010;49(8):3505–15.
[46] Shridhar R, Cooper DJ. A novel tuning strategy for multivariable model predictive control. ISA Trans 1997;36(4):273–80.
[47] Richalet J, ODonovan D. Predictive functional control – principles and industrial applications. Springer; 2009.